

Direct Photon plus Jet Study for CMS

Pooja Gupta¹, B.C.Choudhary², S.Chatterji³, S.Bhattacharya⁴ and R.K. Shivpuri⁵

Department of Physics and Astrophysics, University of Delhi,
Delhi, 110 007, India

Abstract

We present simulation results of $\gamma + \text{Jet}$ analysis using CMS (Compact Muon Solenoid) Object-Oriented software at the LHC center of mass energy ($\sqrt{s}=14$ TeV). The study of direct photon production helps in validating the perturbative quantum chromodynamics (pQCD) and constraining the gluon distribution of nucleons. Direct photon processes also represent a major contribution in estimating background to other Standard Model (SM) processes and signals of new physics. Thus these processes need to be understood precisely in the new energy regime mentioned above. In this work, we have done a detailed study of the complete GEANT4 simulated events of $\gamma + \text{jet}$ generated with Pythia and the related background processes at $\sqrt{s}=14$ TeV. Isolation cuts have been defined for the direct photon which improves the signal to background ratio by $\sim 25\%$ as compared to previous studies done in CMS. The inclusion of a $\Delta\phi$ cut at 40° in the analysis leads to a further increase of $\sim 15 - 17\%$, thus giving an overall gain of $\sim 42\%$ in S/B ratio.

¹Email Address: pooja@fnal.gov

²Email Address: brajesh@fnal.gov

³Email Address: Sudeep.Chatterji@cern.ch

⁴Email Address: bhattacharya.satyaki@gmail.com

⁵Email Address: shiv@fnal.gov

Introduction

The study of physics beyond the Standard Model at Large Hadron Collider (LHC) requires a complete understanding of the QCD processes. Some of the QCD processes constitute major background to other Standard Model (SM) processes, and also to signals of new physics. Thus these processes need to be well understood precisely in the new energy regime. In this work, we have concentrated on the QCD process $pp \rightarrow \gamma^{dir} + 1jet + X$, where X can be anything. This process is a major background to other Standard Model processes such as $H \rightarrow \gamma\gamma$ [1], $W^\pm \rightarrow \pi^\pm\gamma$, and signatures of physics beyond the SM such as Large extra dimensions and SUSY. Inclusive direct photon cross-section was studied at the Tevatron and the region of photon transverse momentum P_T^γ explored by the D0 experiment extends from 23 GeV to 250 GeV. The results from NLO pQCD calculation agrees with the measurement within uncertainties[2].

Direct or prompt photons are photons that emerge directly from the hard scattering of the partons and not from secondary decays or as the radiation product of initial or final state partons. Since these photons come directly from parton-parton hard scattering, they provide a clean signature of the underlying hard scattering dynamics. Prompt photon production in hadronic interactions provides a test of pQCD and a constraint on parton distribution functions (PDFs) of the hadrons. Theoretical investigations have shown[3] that the cross-section for direct photon production has a pseudorapidity (η) dependence which is sensitive to the parameterization of the gluon distributions[4]. The LHC energy will provide an opportunity to determine gluon density in a proton in new kinematic region of x ($2 \times 10^{-4} < x < 1.0$) and Q^2 ($1.6 \times 10^3 - 2 \times 10^5 (GeV/c)^2$)[5]. The analysis of the LHC data in combination with results from the Tevatron and the HERA would allow to extend the QCD analysis in Q^2 region $10^2 < Q^2 < 10^5 (GeV/c)^2$ [6].

For direct photon production, the leading order is defined by two QCD processes; Quark-Gluon Compton scattering, $q+g \rightarrow \gamma^{dir}+q$ and Quark-Antiquark annihilation, $q+\bar{q} \rightarrow \gamma^{dir}+g$. Because of the abundance of low momentum fraction gluons in the proton at LHC energy, Compton scattering is the dominant mechanism contributing to prompt photon production over most of the kinematical region.

Unfortunately, the advantages of photons as a clean probe of parton distributions are offset by large QCD backgrounds which are $\sim 10^3$ to 10^4 times larger than that of direct photon signal. The background contribution to direct photon is mainly caused by the events where high P_T photons are produced in the decays of neutral mesons π^0 , η , k_s^0 and ω^0 , and from events where the photons are radiated from the quark (i.e, bremsstrahlung photons in the next-to-leading order QCD subprocesses such as $qg \rightarrow qg$, $qq \rightarrow qq$ and $q\bar{q} \rightarrow q\bar{q}$). Any analysis must separate true direct photons (those coming from the hard scattering) from those copiously produced in the decays of π^0 , η , k_s^0 , ω^0 and bremsstrahlung photons emerging from high E_T jets. To suppress these backgrounds, we impose isolation cuts on the reconstructed photon candidates. Photon isolation requires the amount of deposited energy in a cone of size R (in pseudorapidity (η) and azimuthal angle (ϕ)) around the photon to be smaller than a particular chosen threshold value. These isolation criteria effectively suppress the background contribution[7]. The purpose of this work is to study the $\gamma + jet$ events and its background

processes with full detector simulation and reconstruction, and optimize the signal/background ratio at the LHC energy.

In this work, we present the GEANT4 simulated results of Level-3 Triggered photons (also called High Level Trigger (HLT) photons) using CMS Software packages. The event generation for $\gamma^{dir} + jet$ signal and background processes has been done using CMKIN[8]. The passage of particles through the detector geometry, showering, energy loss in the calorimeters and reconstruction of the events are modeled in the CMS simulation and reconstruction packages namely, OSCAR[9] and ORCA[10] respectively.

The Physics of $\gamma + jet$

Fig. 1 shows the two leading order (LO) processes namely, “Quark-Antiquark Annihilation” and “Quark-Gluon Compton Scattering” which contributes to $\gamma + jet$ events. In quark-gluon Compton scattering, a gluon scatters from a quark producing a photon in the final state along with the scattered quark. Another way in which photon can be produced is quark-antiquark annihilation, in which the direct photon is produced along with an outgoing gluon.

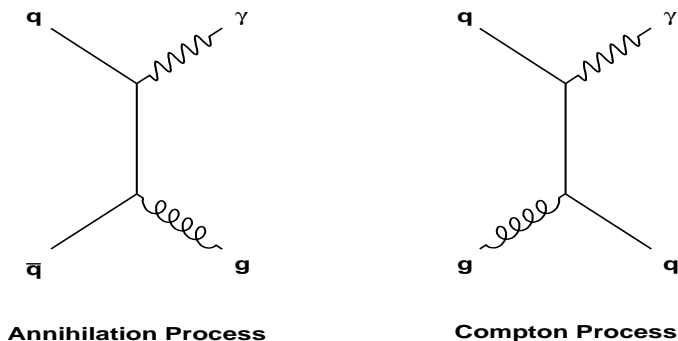


Figure 1: Leading order processes contributing to Direct Photon Events.

An example of a next-to-leading order (NLO) real correction and corresponding virtual corrections (which cancel the soft and collinear divergences arising from the real radiation) are shown in Fig. 2. Only the real corrections (bremsstrahlung diagram) give rise to non back-to-back $\gamma + jet$ topologies with one additional jet. Current direct photon QCD theoretical calculations include only up to the two jet level, of the order α_s^2 , next-to-leading order terms. If the terms beyond the NLO are small, the NLO prediction should be a good approximation to the experimentally measured inclusive cross-section. In the D0 experiment the isolated photon cross-sections were computed to the next-to leading order in α_s using the program JETPHOX[11, 12] with CTEQ6.1M PDF. The renormalization, factorization and fragmentation scales were set to $\mu_{R,F,f} = P_T$. The NLO theory provided a good description of the data over the range, $23 < P_T < 300$ GeV[13].

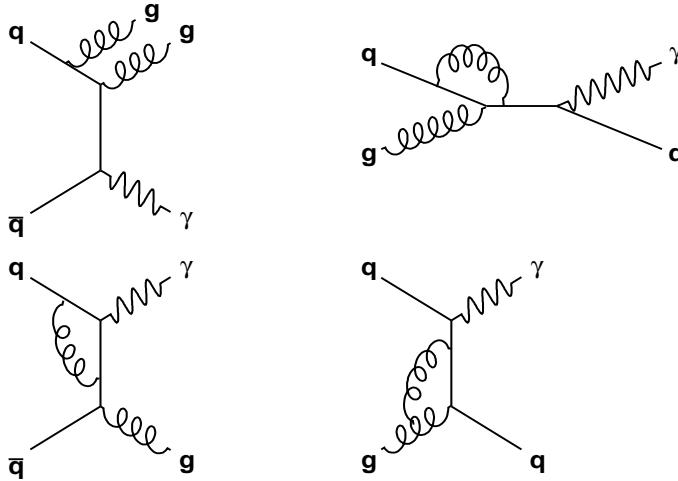


Figure 2: NLO real diagram and corresponding virtual diagrams of Direct Photon Events.

The main background to the direct photon signal comes from jet fluctuations. While most jets consist of many particles, thus easily distinguishable from a single photon, a small fraction ($\sim 10^{-3} - 10^{-4}$) of jets fragment in such a way that a single particle carries most of the momentum of the parent parton. The lightest and therefore most commonly produced neutral meson, the π^0 decays to two photons with a branching ratio of $\sim 99\%$. For high P_T π^0 (and other neutral mesons), the photons produced are very close to each other in the electromagnetic calorimeter forming a single shower thus mimicking a direct photon. Therefore, non-direct photons are common in hadronic collisions. Since jet production rates are $\sim 10^3$ times larger than that of direct photons (depends on $|\eta|$ and P_T), the number of jets which fragment to a single meson and then decay to photons referred to as electromagnetic (EM) jets are comparable to the level of direct photons. The background to direct photon + jet can also come from photons produced in initial and final state radiation. In these cases, the photon is not produced directly from the interaction vertex, and therefore, is not really a direct photon. In order to reduce the background contribution, an isolation criterion is imposed on the photon: typically a cone in η and ϕ around the photon is required to have less than a certain amount of energy. Since a photon produced through bremsstrahlung tends to be collinear with the parent quark (and thus the jet resulting from the quark's subsequent fragmentation), the requirement that the photon be isolated removes all but very large angle radiations. Figures 3 and 4 show major backgrounds to direct photons, namely, the EM jets and the bremsstrahlung.

Monte Carlo Event Generation

At the LHC energy, the cross-sections for the channels $pp \rightarrow \gamma + jet$ and $pp \rightarrow jets$ are very large, thus making it nearly impossible to simulate direct photon signal and its background

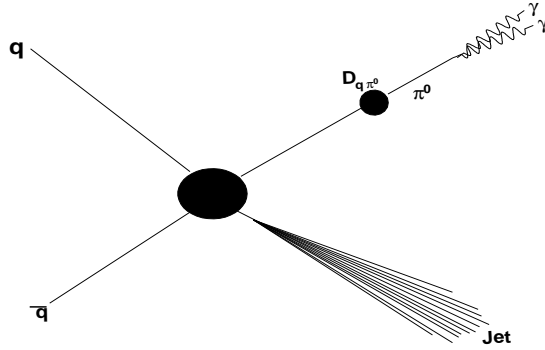


Figure 3: Background contributions to Direct Photon Events from EM jets.

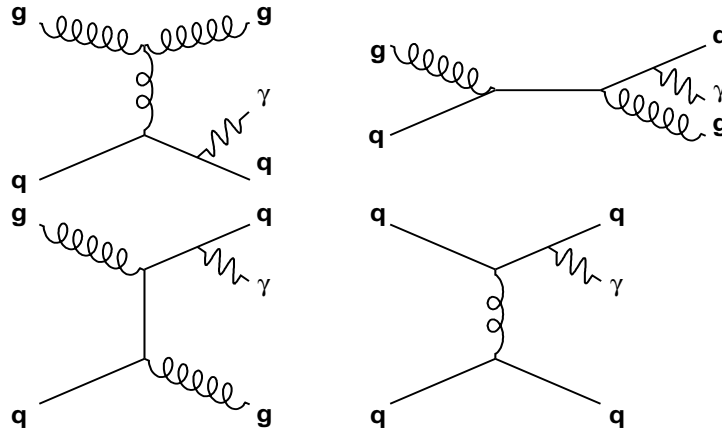


Figure 4: Background contributions to Direct Photon Events from final-state radiation processes.

processes equivalent to an integrated luminosity of $\sim 1fb^{-1}$. In order to achieve this, a selection based on kinematic information of the particle is performed at the generator level which allows only those events that are likely to pass the analysis selection. The geometrical crystal coverage of the Electromagnetic Calorimeter (ECAL) in CMS extends unto $|\eta| = 3.0$. Since the preshower extends upto $|\eta| < 2.6$, in our study we have used the EM coverage upto $|\eta| < 2.6$. In CMS at a luminosity of $2 \times 10^{33}cm^{-2}s^{-1}$, the L1 Trigger P_T cut for a L1 isolated single photon is 23 GeV, while that for the HLT photon it is 80 GeV[15]. For the signal, a pre-selection has been used at the generator level which retains only those events having a direct photon with $P_T^\gamma > 70GeV$ and $|\eta^\gamma| < 2.8$, which are well below the final analysis cut of $P_T^\gamma > 80GeV$ and $|\eta^\gamma| < 2.6$. The Level-1 trigger efficiency for the signal was found to be above 99% over the

entire kinematic range.

For the backgrounds, we have used two different samples of QCD dijet events. The first sample (*jm03b_qcd*) has been simulated in different P_T bins without any generator level pre-selection but has limited statistics. The other sample (*eg03_jets_1e*) has been preselected at the generator level with an enhanced Level-1 trigger efficiency[7]. In this pre-selection, the first step is to look for the seed particles of electromagnetic objects like photons, electrons and positrons, which have $P_T > 5\text{GeV}$ and $|\eta| < 2.7$. Candidate electromagnetic calorimeter trigger tower energies are then estimated by adding energies of all electromagnetic particles found within $\Delta\eta < 0.09$ and $\Delta\phi < 0.09$ from the seed. Trigger tower candidates that lie within $\Delta\eta < 0.2$ and $\Delta\phi < 0.2$ from each other are suppressed and only those with the highest P_T are retained. The Level-1 single photon electromagnetic trigger is simulated by requiring that one such candidate has transverse energy larger than 20 GeV. Events were generated in two different P_T bins: $50\text{GeV} < P_T < 170\text{GeV}$, and $P_T > 170\text{GeV}$. It was found that in $25\text{GeV} < P_T < 50\text{GeV}$ bin, almost no event survives the HLTphoton criteria (discussed later).

The cross-sections, number of events and corresponding integrated luminosity for these samples are shown in Table 1. The samples have been generated using Pythia[16], simulated and reconstructed using OSCAR and ORCA. We require that the leading photon should have $P_T^\gamma > 80$ GeV and $|\eta^\gamma| < 2.6$. The number of events/GeV calculated as a function of photon P_T for the $\gamma + \text{jet}$ signal and its background after P_T and η requirements for 1fb^{-1} integrated luminosity is shown in Fig. 5.

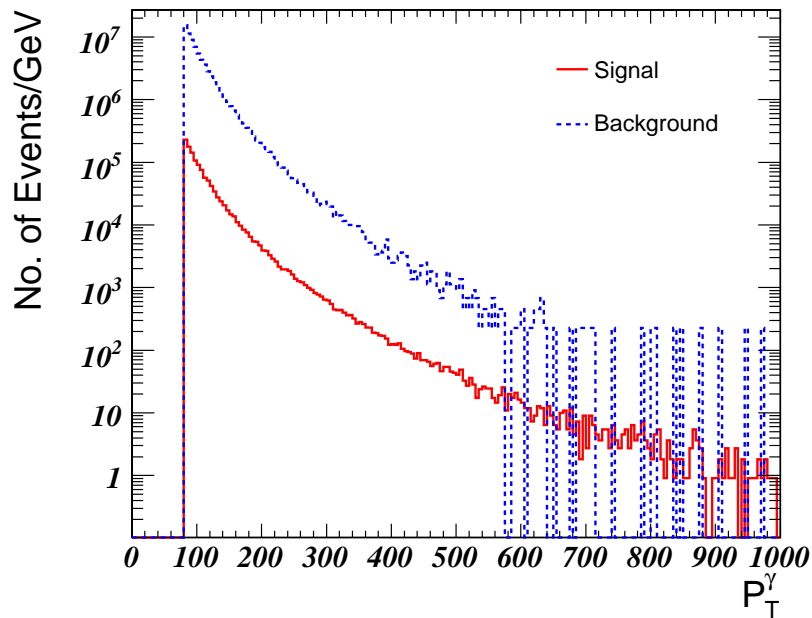


Figure 5: Number of Events/GeV for the $\gamma + \text{jet}$ signal and its background for 1fb^{-1} integrated luminosity at $\sqrt{s}=14$ TeV without any isolation requirements on the photon.

Data Samples	P_T (in GeV)	σ generated (in pb)	σ preselected (in pb)	Number of Simulated Events	Integrated Luminosity (in pb^{-1})
$\gamma + \text{jet}$	50-120	8.53E+03	1.82E+03	30000	16.5
$\gamma + \text{jet}$	120-170	2.77E+02	2.35E+02	12740	54.2
$\gamma + \text{jet}$	170-230	6.76E+01	6.19E+01	11918	192.5
$\gamma + \text{jet}$	230-300	1.90E+01	1.83E+01	11531	630.9
$\gamma + \text{jet}$	> 300	9.07E+00	8.98E+00	9887	1212.3
eg03_jets_1e_50170	50-170	2.43E+07	4.35E+06	2314853	0.53
eg03_jets_1e_170up	> 170	1.34E+05	1.07E+05	473668	4.4
jm03b_qcd_50_80	50-80	2.09E+07	2.09E+07	198993	0.009
jm03b_qcd_80_120	80-120	2.94E+06	2.94E+06	276986	0.094
jm03b_qcd_120_170	120-170	4.99E+05	4.99E+05	247002	0.50
jm03b_qcd_170_230	170-230	1.01E+05	1.01E+05	50000	0.50
jm03b_qcd_230_300	230-300	2.38E+04	2.38E+04	50000	2.09

Table 1: Cross-sections, number of simulated events, and equivalent integrated luminosity for $\gamma + \text{jet}$ events and its background MC samples.

Photon Isolation

All events have been reconstructed using ORCA version 8.7.3. In the electromagnetic calorimeter, the Hybrid and Island clustering algorithms were used to construct basic clusters in the barrel and the endcap respectively. A supercluster is formed by clustering basic clusters, to reconstruct the energy of the electrons which bremsstrahlung within the tracker and the photons that are converted within the tracker. A photon candidate is associated with each reconstructed supercluster. As has already been shown in Fig. 5, jets misidentified as photons give a very large background to the direct photon signal. Isolation cuts are used to reject photons coming from the fragmentation of jets which can mimic the direct photon signal in the detector by

detecting fragments of the other jet which accompany them.

Tracker Isolation

In most of the jet events, a photon candidate is accompanied by charged particles which makes tracker isolation an important parameter in differentiating the signal from the background events. The tracker isolation criteria is based on the number of charged particle tracks with P_T greater than some threshold, P_T^{Thres} , calculated in a cone R ($R = \sqrt{(\Delta\eta^2 + \Delta\phi^2)}$) around the photon candidate. The algorithm contains following three parameters:

1. Cone size R: The size of the cone R around the photon candidate, wherein the number of charged tracks is counted.
2. P_T threshold (P_T^{Thres}): Only charged particle tracks with P_T greater than P_T^{Thres} are considered for photon isolation.
3. Number of tracks threshold (N_{TK}^{Thres}): If the number of charged particle tracks in cone R with P_T greater than the chosen P_T^{Thres} is greater than N_{TK}^{Thres} , then the photon candidate is considered non-isolated, otherwise it is considered as an isolated photon.

The effect of threshold P_T value (P_T^{Thres}) for the track on signal efficiency and the background rates have been investigated. The effect of varying the number of tracks allowed (N_{TK}^{Thres}) have been studied on the signal efficiency and the background rates. Both these studies were performed for the barrel and the endcaps with various cone sizes. For a particular cone size and track P_T , we determined the signal efficiency as a function of background rate. These values are determined for different values of N_{TK}^{Thres} from 4 to 0. This yields a curve of the form shown in Fig. 6(a), which shows the distribution for cone size $R = 0.3, 0.4$ and track $P_T > 1.0, 1.5$ and 2.0 GeV for the barrel region. Fig. 6(b) shows the same distribution for the cone sizes 0.5 and 0.7 . Figures 7 (a) and (b) show the same distribution for various cone sizes in the endcaps. The (N_{TK}^{Thres}) value is varied in steps of 1. It can be seen from the figures that the background rate is very sensitive to the N_{TK}^{Thres} value. By increasing N_{TK}^{Thres} from 0 to 1, one can improve the signal efficiency by 4-10% while the background rate increases by a factor of ~ 2 in the barrel and ~ 1.5 in the endcaps. Therefore, the parameter N_{TK}^{Thres} is fixed to be equal to zero. The increase in cone size leads to a large drop in overall background rates but at the cost of signal efficiency. The performance of the tracker variables is not as good in endcaps due to larger tracker inefficiencies. For a fixed cone size, both signal efficiency and background rate increase with increase in track P_T threshold, P_T^{Thres} . Different values of P_T^{Thres} for different cone sizes have been taken into account to estimate the optimized signal to background ratio.

Electromagnetic Calorimeter Isolation

The ECAL isolation criteria are based on the sum of transverse energies deposited in the basic clusters in some cone of radius R in $\eta - \phi$ plane around a photon candidate. The basic clusters

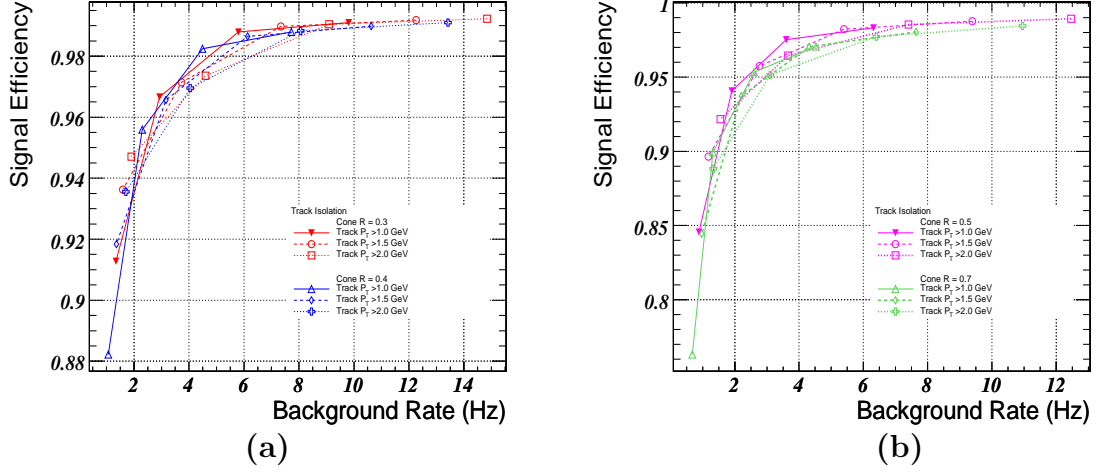


Figure 6: Performance of the tracker isolation variables in the barrel for various cone sizes $R = 0.3$ and 0.4 (a); $R = 0.5$ and 0.7 (b) for different track P_T^{Thres} .

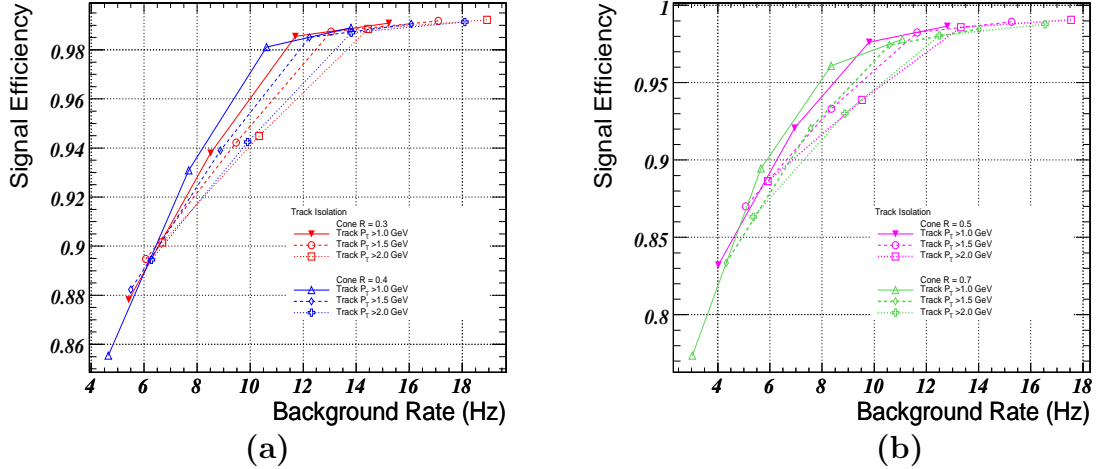
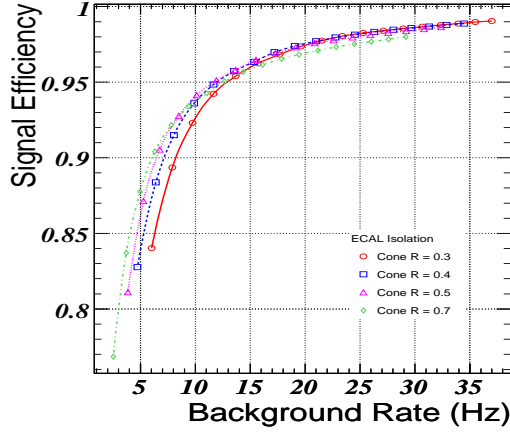


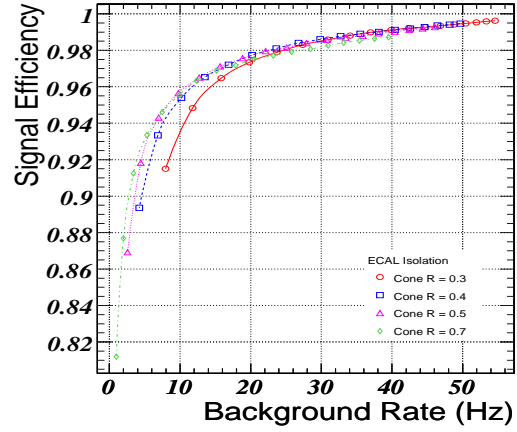
Figure 7: Performance of the tracker isolation variables in the endcaps for various cone sizes $R = 0.3$ and 0.4 (a); $R = 0.5$ and 0.7 (b) for different track P_T^{Thres} .

that belong to the photon candidate supercluster are not counted as a part of the sum. If the sum of transverse energies (ΣE_{TECAL}) is below threshold value (E_{TECAL}^{Thres}), the photon candidate is considered isolated, otherwise it is considered non-isolated.

The effect of making the values of E_{TECAL}^{Thres} increasingly stringent and their dependence on the signal efficiency as well as on background rate for different cone sizes R can be seen in figures 8 (a) and (b) respectively for the barrel and the endcaps. The value of E_{TECAL}^{Thres} is gradually decreased from a very large value in steps of 0.5 GeV to yield the curves. Just to illustrate

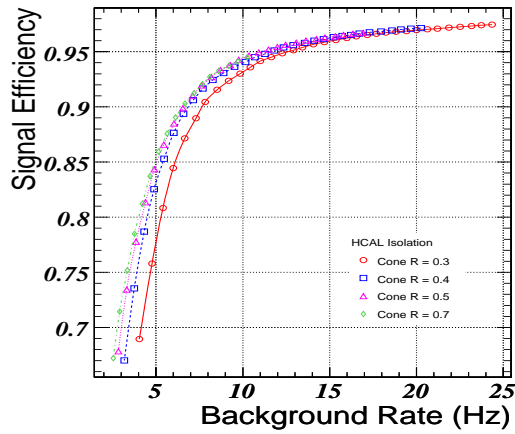


(a)

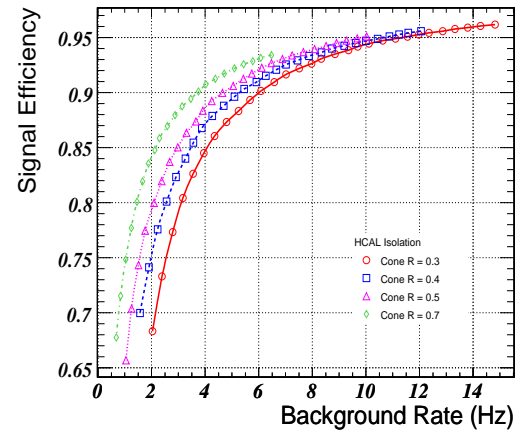


(b)

Figure 8: Performance of the variable E_{TECAL} for various cone sizes $R = 0.3, 0.4, 0.5$ and 0.7 for the barrel (a) and for endcaps (b).



(a)



(b)

Figure 9: Performance of the variable E_{THCAL} for various cone sizes $R = 0.3, 0.4, 0.5$ and 0.7 for the barrel (a) and for endcaps (b).

the nature of dependence of the signal efficiency and background rates, the plots shown have variation in E_{TECAL}^{Thres} from 17 GeV to 1 GeV. The stringent selection cut on ΣE_{TECAL} provides a good background rejection. In the endcaps, a higher stringent cut as compared to that in barrel region can further enhance background reduction.

Hadron Calorimeter Isolation

The hadronic activity around the background photons tends to be much more than around the direct photons. Thus, the HCAL isolation can also be used for photon selection. For isolation in HCAL, the sum of transverse energies of all the particles depositing energy in the HCAL is calculated in a cone of size R around a photon candidate. If the sum of transverse energies of the hadronic particles, ΣE_{THCAL} is below a certain threshold value (E_{THCAL}^{Thres}), the photon candidate is considered isolated. As the information from the charged mesons and hadrons is also exploited in the tracker, the HCAL offers partially redundant information.

Following the above procedure for ECAL isolation, the effect of making the E_{THCAL}^{Thres} more stringent and its dependence on the signal efficiency and the background rate is shown in figures 9 (a) and (b) respectively for the barrel and the endcaps. The E_{THCAL}^{Thres} is gradually decreased from a very large value in steps of 0.5 GeV to yield the curves. The HCAL isolation variable offers a better background rejection in the endcaps.

Combination of the Detectors

After studying the isolation parameters separately, the task is to combine their effects such that the signal to background ratio is maximized. This study has been done for the various detector combinations (Tracker + HCAL, Tracker + ECAL, Tracker + ECAL + HCAL) for different threshold parameters. We observe that a better reduction in the background rate without compromising the signal efficiency can be achieved by combining isolation requirements from various detectors. Some combinations which are found to yield better signal to background ratio are shown in Table 2 and the respective overall signal efficiency and rates obtained are shown in Table 3. It should be noted that the selection cut A has been used in the results mentioned in CMS Physics TDR-I[15]. With selection cut C, the background rate is further reduced by $\sim 22\%$ with only one percent decrease in the signal efficiency, thus giving a $\sim 26\%$ increase in the S/B ratio. Using selection cut C, the number of events/GeV for $1 fb^{-1}$ integrated luminosity calculated as a function of photon P_T for the $\gamma + jet$ signal and its background is shown in Fig. 10. The effect of the isolation criteria on the number of events/ GeV can be observed by comparing Fig. 5 and Fig. 10.

Selection Cut	Cone Size R	E_{TECAL}^{Thres} (GeV)	E_{THCAL}^{Thres} (in Barrel)(GeV)	E_{THCAL}^{Thres} (in Endcaps)(GeV)	P_T^{Thres} (GeV)
A	0.3	1.5	6.0	4.0	1.5
B	0.3	1.5	6.0	5.0	1.0
C	0.4	2.0	7.0	5.0	1.5
D	0.4	2.0	6.5	5.0	1.5
E	0.5	2.5	8.0	6.0	1.5

Table 2: Selection Cuts corresponding to the different values of the isolation threshold parameters.

Selection Cut	Signal Efficiency	Signal Rate (Hz)	Background Rate (Hz)	S/B Ratio
A	0.76	2.12	1.40	1.52
B	0.76	2.10	1.26	1.66
C	0.74	2.09	1.09	1.92
D	0.73	2.07	1.06	1.94
E	0.70	1.99	0.84	2.37

Table 3: Signal efficiency, signal and background rates for low luminosity at $\sqrt{s}=14$ TeV.

Fig. 11 shows the the predictions for the differential cross-section of the $\gamma + 1$ jet events as a function of P_T^γ compared with theoretical LO and NLO calculations[17]. The error bars on the x-axis represents the bin width. The differential cross-section calculated from the simulated data is represented as LO (calculated after full simulation) in the above mentioned figure. To evaluate it, the cross-section from Pythia was generated using CTEQ5L parton distribution function and renormalization scale $\mu = P_T$. Various factors like efficiency of the analysis cuts, Luminosity, geometrical acceptance have been taken into account. The theoretical LO and NLO calculations are those provided by Owens[18]. The results are found to be in agreement with the theoretical LO calculations. We see that the NLO QCD contribution is higher than the LO in the whole P_T range under analysis.

$\Delta\phi$ cut

In $\gamma +$ jets events, the jets have been reconstructed using Iterative Cone type algorithm with cone size $R = 0.5$ [19]. Since the HCAL extends up to $|\eta| < 5.0$ the selection cuts used on the highest P_T jet are : $P_T^{jet} > 40 GeV$ and $|\eta^{jet}| < 5.0$. Usually $\gamma + 1$ jet events are produced in a “back-to-back” fashion, but this topology is disturbed by initial-state and final-state radiation. The events with the vector P_T^{jet} being “back-to-back” to the vector P_T^γ within $\Delta\phi$ can be defined by the equation;

$$\Phi(\gamma, jet) = 180^\circ \pm \Delta\phi$$

where $\Phi(\gamma, jet)$ is the angle between P_T^γ and P_T^{jet} vectors. We have studied the effect of $\Delta\phi$ cut after applying all photon isolation requirements to see if we get any further enhancement in the S/B ratio while retaining a very high signal efficiency. The performance plot of the $\Delta\phi$ as the function of signal efficiency is shown in Fig. 12. It shows the variation in signal efficiency with the change in $\Delta\phi$ for all the selection cuts given in Table 2. In Fig. 12, we also show the performance of $\Delta\phi$ as a function of signal efficiency vs. signal to background ratio for all selection cuts noted in Table 2 where $\Delta\phi$ is varied in steps of 5° . It is found that the limit $\Delta\phi < 40^\circ$ can be used as an additional cut to improve the S/B ratio. In all cases this cut increases the S/B ratio by $\sim 15 - 17\%$ with a bare reduction of $1 - 2\%$ in signal efficiency.

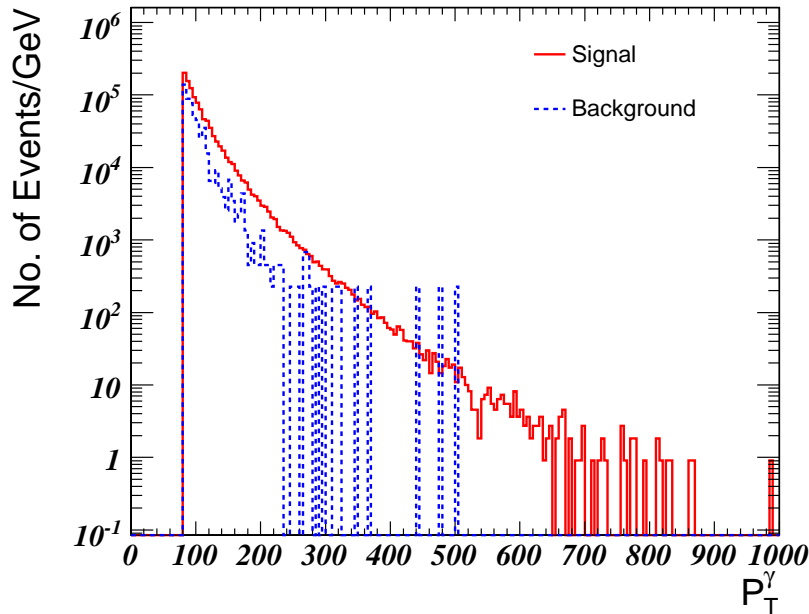


Figure 10: Number of Events/GeV for the γ + jet signal and its background for $1 fb^{-1}$ integrated luminosity at $\sqrt{s}=14$ TeV after applying the selection cut C.

Statistical and Systematic errors

The statistical error on the signal and the background rates are found to be $\sim 1\%$ and $\sim 5\%$ respectively.

The following potential theoretical and experimental sources of systematic error have been considered:

1. PDF uncertainties: We have used the CTEQ 6 PDF sets from the LHAPDF package [20] to determine the pdf uncertainties with respect to CTEQ 6M PDF (the global minimum of χ^2 of the CTEQ 6 set)[21]. The error in the signal cross-section was found to be $\sim 3-4\%$ and the variation in the background is $\sim 5-7\%$. This results in a rate variation of $\sim 3\%$ for the signal and $\sim 5\%$ for the background.
2. Uncertainty due to scale variation: The uncertainty in scale variation was estimated by determining the cross-section for different available choices of hard scale in Pythia[15]. The largest variation from default choice of Q^2 was observed when $Q^2 = \hat{s}$ (MSTP 32=4). The signal varies from 4–13% with increasing P_T while the background changes by $\sim 27\%$ resulting in rate variation of $\sim 7\%$ for the signal and $\sim 27\%$ for the background.
3. Luminosity error: In initial phase of LHC operation for an integrated luminosity of $1fb^{-1}$, the error on the measured luminosity at CMS is expected to be $\sim 10\%$ [15].

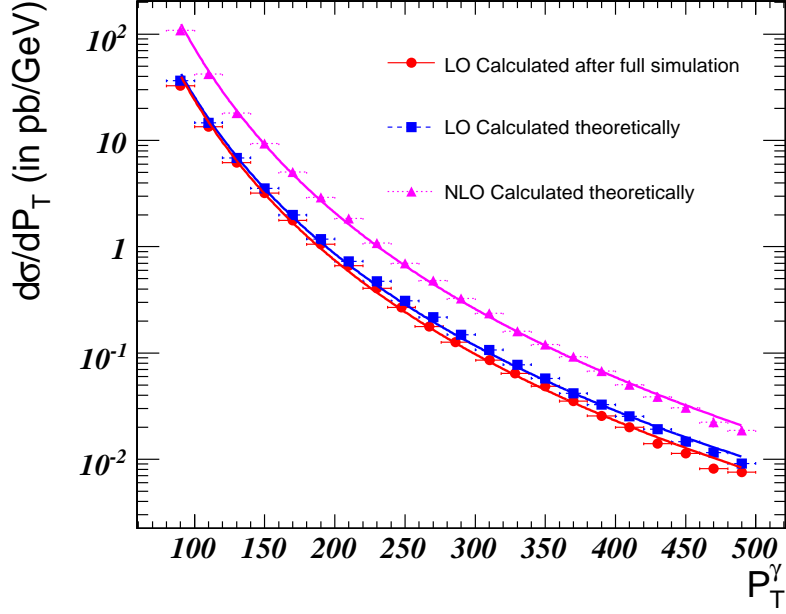


Figure 11: The LO (after full simulation) and theoretical LO and NLO calculations for the cross-section of $\gamma + \text{jet}$ events as a function of P_T^γ . The calculated points have been complemented by lines fitting the corresponding cross sections.

4. Photon trigger: The systematic error arising from the photon triggers is expected to be of the order of $\sim 1\%$ [1, 22].
5. Photon energy scale: To estimate the error the photon energy in each event was scaled up and down by 0.05% [23] and the corresponding error on the rate was found to be $+0.25\%$ -0.16% for the signal and $\pm 0.34\%$ for the background.
6. Jet energy scale: The uncertainty was determined by scaling the jet energy by 10% for $P_T < 20\text{GeV}$, by linearly scaling from 20 GeV onward and by 3% at high P_T [15]. For jets having $P_T^{\text{jet}} > 40\text{GeV}$, it has been estimated to be $\pm 0.4\%$ for the signal and $+0.7\%$ -0.3% for the background. If the selection criterion is changed to $P_T^{\text{jet}} > 60\text{GeV}$, the observed effect is $\sim \pm 7\%$ as the number of events having jets and a single isolated photon is larger in $40\text{GeV} < P_T^{\text{jet}} < 60\text{GeV}$ bin as compared to lower P_T^{jet} bins.
7. Jet energy resolution: To estimate the systematic uncertainty due to jet energy resolution, an event by event smearing of the jet energy was done such that the σ_{P_T} changes by 10%[15]. The corresponding error on the rate was calculated to be 0.3% for the signal and 1% for the background.
8. Preselection efficiency : The systematic uncertainty arising from the preselection efficiency was found to be less than 3% for both the signal and the background.

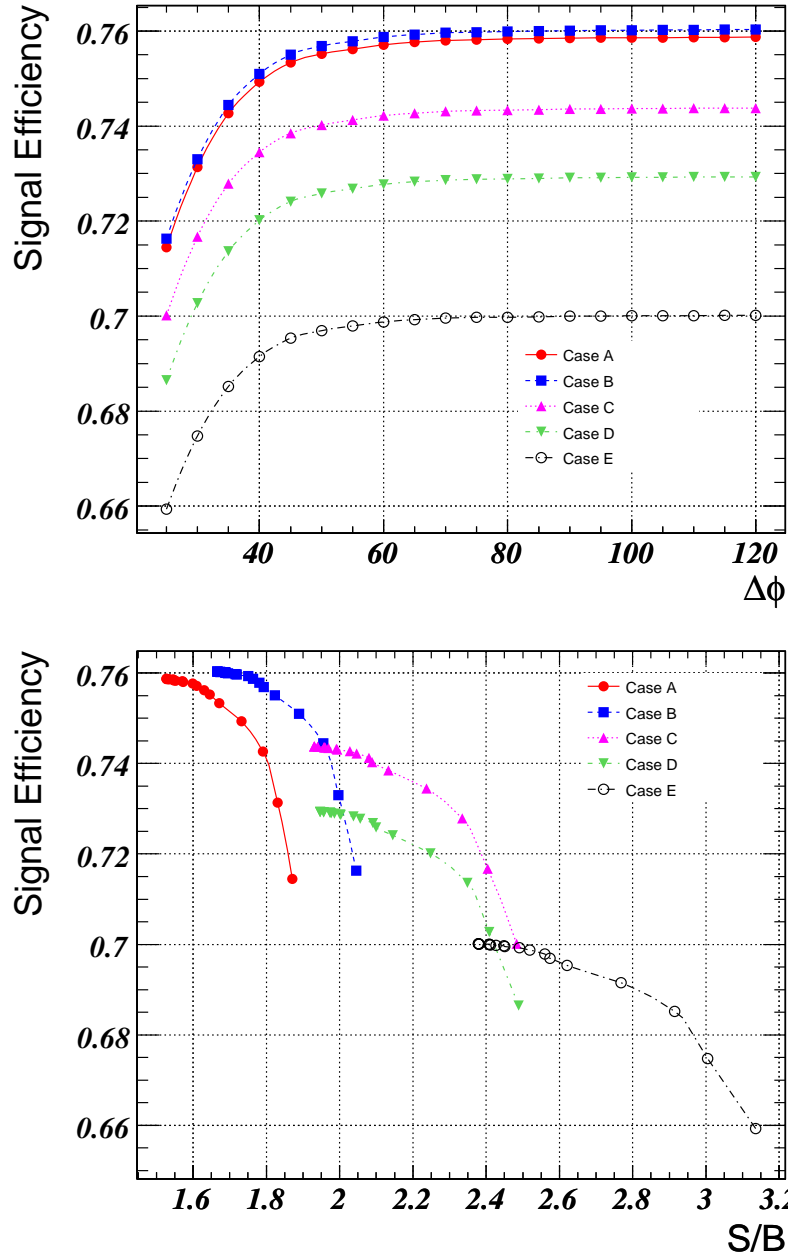


Figure 12: Performance of the $\Delta\phi$ variable for various selection cuts (Table 2) as a function of Signal efficiency (up) and signal efficiency vs. S/B ratio (down).

Several of the uncertainties mentioned above such as luminosity, photon trigger, etc. will cancel out in the measurement of the S/B ratio. The uncertainties arising from the theoretical systematics (such as PDF, scale variation) being unequal for the signal and the background will

not lead to complete cancellation. Here we have not considered some other sources of systematic uncertainties which could be significant. The higher order perturbative QCD corrections which are different for the signal and the background, can have significant uncertainty. The large uncertainties arising from the non-perturbative fragmentation models used in the simulation and efficiency of selection may also affect the background rate. In simulation we have not taken into account the uncertainties coming from shower shape modelling and conversions which would be known once the real data is available. The HERA experiment has studied the systematic errors due to possible imperfections in the simulation of the shower shapes which resulted in errors on the direct photon cross-section from ± 10 to $\pm 20\%$ [24]. The CDF experiment studied the direct photon cross-section with conversions and reported the uncertainty on the cross-section measurement due to total conversion probability as $+28\%$ and -18% [25]. The D0 experiment reported uncertainties on photon cross-section measurements due to photon conversions as 3% , due to photon purity as 3.0% and due to event vertex determination as $3.6 - 5.0\%$ [2]. Since in CMS too the photon conversion rate is high[14], it is possible that the systematics due to conversion probability could be significant. Taken together these systematics may result in large uncertainty on the estimated rates. Since many of these systematics can only be properly estimated using the CMS data, our educated estimate is that the total systematics can vary from 15% to 25% , as many of them are experiment and detector dependent. As more and more data will be accumulated, beam and detector response will be better understood and one expects to reduce the systematics to the level of $10 - 15\%$.

Conclusions

In this analysis, we have explored the direct photon + jet production in the region of photon transverse momentum (P_T^γ) from HLT P_T threshold of 80 GeV to a few hundred GeV. We have studied the ECAL, HCAL and the tracker based isolation conditions for the direct photon physics. For low luminosity phase of the LHC operation, it is found that with optimized isolation conditions the background can be reduced by two orders of magnitude while the signal efficiency remains between $70\% - 80\%$. Isolation requirement within a larger cone around a photon provides a clean and pure signal. It is found that for the entire P_T range in the analysis, carefully chosen values of the isolation threshold parameters can yield appreciable increase in the S/B ratio as compared to previous studies while retaining very high signal efficiency. We have found the selection cut C (Table 2) to be optimum. We have matched our results from the Pythia based simulation with an independent theoretical calculation and they are found to be in excellent agreement. The topology of the $\gamma + \text{jet}$ events is such that at high P_T most of the direct photon and jet events are "back to back" within certain $\Delta\phi$. The inclusion of a very wide $\Delta\phi$ cut at 40° in the analysis leads to a further increase of $\sim 15 - 17\%$ thus leading to an overall gain $\sim 42\%$ in S/B ratio. A better understanding of fake photon rejection will naturally lead to improved efficiency for detecting low mass Higgs decaying to photon pairs.

Acknowledgments

We are grateful to J. Owens for his assistance with the NLO theoretical calculations. We thank M. Pieri for helping us with the background samples. We also wish to express thanks to P. Demin, D. Futyan, M. Mangano, C. Seez and R. Y. Zhu. The work has been supported by a grant from the Department of Science and Technology, Govt. of India. Pooja Gupta would also like to thank the Council of Scientific and Industrial Research (CSIR), India for providing financial assistance.

References

- [1] M. Pieri et al., “Inclusive search for the Higgs Boson in the $H \rightarrow \gamma\gamma$ channel”, *CMS NOTE-2006/112* (2006).
- [2] V.M. Abazov et al., “Measurement of the Isolated Photon Cross Section in p-pbar Collisions at $\sqrt{s}=1.96$ TeV”, *Phys. Lett. B* **639** (2006) 151-158.
- [3] P. Aurenche et al., “Prompt photon production at colliders”, *Phys. Rev. D* **Vol 42, No. 5** (1990) 1440-1449.
- [4] E.C. Reid, H. F. Heath, “Direct Photon in CMS”, *CMS NOTE-2000/063* (2000).
- [5] D.V. Bandourin, V.F. Konoplyanikov, “On the application of photon+jet events for setting the absolute jet energy scale and determining the gluon distribution at the LHC”, *arXiv:hep-ex/0207028 v2* (2002).
- [6] D.V. Bandourin, N.B. Skachkov, “On the application of photon+jet events for setting the absolute jet energy scale and determining the gluon distribution at the LHC”, *arXiv:hep-ex/0403024 v1* (2004).
- [7] L. Agostino, M. Pieri, “High Level Trigger Selection of Electrons and Photons”, *CMS NOTE-2006/078* (2006).
- [8] CMKIN, “CMS Interface for Event Generator”, <http://cmsdoc.cern.ch/cmsoo/projects/CMKIN>.
- [9] OSCAR, “Object-oriented Simulation for CMS Analysis and Reconstruction”, <http://cmsdoc.cern.ch/OSCAR>.
- [10] ORCA, “Object-oriented Reconstruction for CMS Analysis”, <http://cmsdoc.cern.ch/orca>.
- [11] T. Binoth, J.P. Guillet, E. Pilon and M. Werlen, “A full next-to-leading order study of direct photon pair production in hadronic collisions”, *Eur. Phys. J. C* **16** (2000) 311.
- [12] S. Catani, M. Fontannaz, J.P. Guillet, E. Pilon, “Cross section of isolated prompt photons in hadron-hadron collisions”, *JHEP* **0205** (2002) 028.

- [13] M. Wobisch (on behalf of the CDF and D0 collaborations), “Photon Cross Sections at $E_{cm} = 2$ TeV”, Presented at XLIRST Rencontres de Moriond on “QCD and High Energy Hadronic Interactions” La Thuile, Italy, March 18-25, 2006 *arXiv:hep-ex/0606063 v1* (2006).
- [14] CMS Collaboration “CMS ECAL Technical Design Report”, *CERN/LHCC 97-33* (1997).
- [15] CMS Collaboration, “CMS Physics Technical Design Report Volume I”, *CERN/LHCC 2006-001* (2006).
CMS Collaboration, “CMS Physics Technical Design Report Volume II”, <http://cmsdoc.cern.ch/cms/cpt/tdr>.
- [16] T.Sjostrand and P. Z.Skands, “Transverse-Momentum-Ordered Showers and Interleaved Multiple Interactions”, *arXiv:hep-ph/0408302 v1* (2004).
- [17] H. Baer, J. Ohnemus, J.F. Owens, “Next-to-leading-logarithm calculation of direct photon production”, *Phys. Rev. D* **Vol 42** (1990) 61.
- [18] Jeff Owens *Private Communications*.
- [19] CMS Collaboration, “The Tridas Project Design Report, Volume 2: Data Acquisition and High-Level Trigger”, *CERN/LHCC 2002-26* (2002).
- [20] M. R. Whalley, D. Bourilkov, and R. C. Group, “The Les Houches Accord PDFs (LHAPDF) and Lhaglu”, *arXiv:hep-ph/0508110* (2005).
- [21] P. Bartalini, R. Chierici, A. De Roeck, “Guidelines for the Estimation of Theoretical Uncertainties at the LHC”, *CMS NOTE-2005/013* (2005).
- [22] S. Baffioni et al., “Discovery potential for the SM Higgs boson in the $H \rightarrow ZZ \rightarrow e^+e^-e^+e^-$ decay channel”, *CMS NOTE-2005/115* (2005).
- [23] P. Meridiani, R. Paramatti, “Use of $Z \rightarrow e^+e^-$ events for ECAL calibration”, *CMS NOTE-2006/039* (2006).
- [24] H1 Collaboration, “Measurement of Prompt Photon Cross-sections in Photoproduction at HERA”, *arXiv:hep-ph/0407018 v1* (2004).
- [25] CDF Collaboration, “Direct Photon Cross-section with conversions at CDF”, *arXiv:hep-ph/0404022 v2* (2004).